Journal of ELECTRONIC MATERIALS, Vol. 46, No. 1, 2017
DOI: 10.1007/s11664-016-4956-9

Transparent Conductive ITO/Ag/ITO Electrode Deposited at Room Temperature for Organic Solar Cells

JUN HO KIM,[1] TAE-WOON KANG,[2] SUNG-NAM KWON,[2] SEOK-IN NA,[2] YOUNG-ZO YOO,[3] HYEONG-SEOP IM,[1] and TAE-YEON SEONG[1,4]

1.—Department of Materials Science and Engineering, Korea University, Seoul 02841, Korea. 2.—Professional Graduate School of Flexible and Printable Electronics, Chonbuk National University, Jeonju, Jeollabuk-do 54896, Korea. 3.—Duksan Hi-Metal Co. Ltd., Yeonam-dong, Buk-gu, Ulsan 44252, Korea. 4.—e-mail: tyseong@korea.ac.kr

We investigated the optical and electrical properties of room-temperature-deposited indium-tin-oxide (ITO)/Ag (19 nm)/ITO multilayer films as a function of ITO layer thickness. The optical and electrical properties of the ITO/Ag/ITO films were compared with those of high-temperature-deposited ITO-only films for use as an anode in organic solar cells (OSCs). The ITO/Ag/ITO multilayer films had sheet resistances in the range 5.40–5.78 Ω/sq, while the ITO-only film showed 14.18 Ω/sq. The carrier concentration of the ITO/Ag/ITO films gradually decreased from 2.01×10^{22} to 7.20×10^{21} cm^{-3} as the ITO thickness increased from 17 nm to 83 nm. At 530 nm, the transmittance of the ITO/Ag/ITO (50 nm/19 nm/50 nm) films was ~90%, while that of the ITO-only film gave 96.5%. The multilayer film had a smooth surface with a root mean square (RMS) roughness of 0.49 nm. Poly (3-hexylthiophene) (P3HT):[6,6]-phenyl-C61 butyric acid methylester (PCBM) bulk heterojunction (BHJ)-based OSCs fabricated with the ITO/Ag/ITO (50 nm/19 nm/50 nm) film showed a power conversion efficiency (PCE) (2.84%) comparable to that of OSCs with a conventional ITO-only anode (3.48%).

Key words: ITO, Ag, multilayer, transparent conducting electrode, organic solar cell

INTRODUCTION

Organic solar cells (OSCs) based on a polymer-fullerene composite active layer have attracted a great deal of interest for their applications in next generation photovoltaic devices because of their low fabrication cost, light weight, flexibility, and printing-based simple process.[1–3] In particular, bulk-heterojunction OSCs fabricated with a mixture of poly(3-hexylthiophene) (P3HT) and [6,6]-phenyl-C_{61} butyric acid methyl ester (PCBM) were extensively investigated, and their power conversion efficiency (PCE) was shown to reach up to ~3%.[4,5] To increase the PCE of OSCs, anodes should be designed to have a low resistivity and a high transmittance that is required to maximize the absorption of photons. Particularly, the PCE of large-area OSCs is sensitively dependent on the series resistance of anode materials, namely, their electrical and interfacial properties.[6–9] So, the development of high-quality transparent conducting oxide (TCO) films is crucial to the improvement of the performances of OSCs. Currently, radio-frequency (RF)/direct current (DC) sputtering- or ion plating-grown Sn-doped In_2O_3 (ITO) films are the most commonly used transparent anodes for OSCs because they have low resistivities (~10^{-4} Ω-cm), high optical transmittances (~83% at 550 nm), and relatively high work functions (~4.8 eV).[10] Despite their excellent electrical and optical properties, however, conventionally used ITO electrodes have a drawback of using high process temperatures (higher than 300°C) that are required to obtain crystalline ITO phase, lower resistivity, and high transmittance.[11,12] However, for the fabrication of

(Received May 31, 2016; accepted September 9, 2016; published online September 21, 2016)

flexible OSCs on polyethylene terephthalate (PET) substrate or the low-cost fabrication process of OSCs, high process temperatures must be avoided. Thus, for the fabrication of high-performance and low-cost OSCs and/or flexible applications, it is very important to develop a low-temperature-grown TCO electrode with low resistivity and high transmittance that are comparable to those of high-temperature-grown crystalline ITO. For this reason, the dielectric/metal/dielectric (D/M/D) multilayer structures[13–16] have been widely investigated to develop an alternative to crystalline ITO. For example, Kim et al.[17] investigated the effect of Ag layer thickness on the physical properties of ITO/Ag/ITO multilayer films and showed that the ITO/Ag/ITO (43 nm/16.1 nm/43 nm) multilayer films produced good transmittance (79.4% at 550 nm) and low sheet resistance (8.9 Ω/sq.). Choi et al.[18] investigated the opto-electrical and structural properties of ITO and Ag layers as a function of RF powers and deposition temperatures. They reported that ITO/Ag (14 nm)/ITO had a resistance as low as 4 Ω/sq and a transmittance of 90% at 550 nm when ITO films were grown 55–60 nm thick at 200°C. Kim et al.[19] investigated the opto-electrical properties of ITO/Ag/ITO (50 nm/17 nm/50 nm) multilayer films deposited on PET substrates and showed that they gave a sheet resistance of 6.7 Ω/sq. and a transmittance of 83.2% at 550 nm. Kim et al.[20] also investigated the electrical and optical characteristics of ITO/Ag/ITO films (35 nm/8 or 12 nm/35 nm). They reported that ITO/Ag (8 nm)/ITO multilayer had a sheet resistance of 8.9 Ω/sq. and a transmittance of 85.10%, while ITO/Ag (12 nm)/ITO multilayer showed a sheet resistance of 4.4 Ω/sq. and a transmittance of 85.27%. OSCs fabricated with a laser-patterned ITO/Ag/ITO multilayer yielded PCEs of 3.12 and 2.85%, where the Ag thickness was 8 nm and 12 nm, respectively. In our previous work, we investigated the electrical characteristics of inverted OSCs based on P3HT: PCBM bulk heterojunctions (BHJ) fabricated with optimized ZnO/Ag/ZnO multilayer.[21] The ZnO/Ag/ZnO multilayer films showed lower sheet resistances (3.6–3.9 Ω/sq) than ITO 14.2 Ω/sq, and the ZnO/Ag/ZnO (40 nm/19 nm/40 nm) film had a transmittance of $\sim$ 95% at 550 nm, which is comparable to that of ITO ($\sim$96%). OSCs fabricated with the ZnO/Ag/ZnO (40 nm/19 nm/40 nm) film showed a PCE of 2.63% that is comparable to that of OSCs with a conventional ITO cathode (2.71%). In this study, we investigated the optical and electrical properties of ITO/Ag/ITO multilayer films as a function of ITO thickness and compared them with those of commercial ITO-only film. It should be noted that the reference ITO-only film was deposited at 270°C by a company using an RF sputtering system. However, ITO/Ag/ITO films were deposited at room temperature. Haacke's figure of merit (FOM) was calculated to characterize the performance of the multilayers. OSCs were fabricated with ITO-only and ITO/Ag/ITO electrodes and their electrical and optical properties were characterized.

EXPERIMENTAL PROCEDURES

ITO/Ag/ITO multilayer thin films were sequentially deposited on Corning Eagle XG glass substrates at room temperature by an RF magnetron sputtering system. Ceramic ITO (99.999% purity) and pure Ag (99.99% purity) targets were used under a base pressure of less than 1×10^{-6} Torr. Before being loaded into the sputtering chamber, the glass substrate (1.5×1.5 cm^2) was cleaned with acetone, methanol, and deionized water for 15 min per cleaning agent in an ultrasonic bath, and finally dried in a N_2 stream. Prior to deposition, both the ITO and Ag targets were pre-sputtered for 30 min to remove contaminants. ITO and Ag were deposited using RF powers of 90 W and 30 W, respectively. During sputtering, the glass substrates were constantly rotated at a speed of 12 rpm for ITO and 27 rpm for Ag. The thickness of an Ag layer was fixed at 19 nm and those of upper and lower ITO layers varied from 17 nm to 83 nm. Hall measurements by the van der Pauw technique were carried out with a magnetic field of 0.55 T (HMS 3000, Ecopia). The four-point-probe technique was used for measuring sheet resistance. Transmittance of the multilayers was measured with a ultraviolet (UV)/visible spectrometer (UV-1800, Shimadzu). The crystal structure of the multilayers was determined with x-ray diffraction technique (XRD; ATX-G, Rigaku). In addition, the surface morphology of the multilayer films was assessed using an atomic force microscopy (AFM) system (XE-100, Park systems).

P3HT:PCBM-based BHJ-based OSCs were fabricated with optimal ITO/Ag/ITO films, and their electrical performance was compared with that of OSCs with reference ITO films. Figure 1 shows schematic diagrams of OSCs that are composed of glass substrate, a transparent electrode (ITO or ITO/Ag/ITO), a hole transport layer (HTL) [poly(3,4-ethylenedioxythioph-ene):poly(styrenesulfonate), PEDOT:PSS], an active layer (P3HT:PCBM), and cathode (Ca/Al) electrode. Prior to the fabrication of OSCs, optimal ITO/Ag/ITO and conventional ITO-coated glass samples were consecutively cleaned by mucasol, acetone, isopropanol, and de-ionized water, followed by UV/ozone treatment for 10 min. Note that the conventional ITO (150 nm thick) on substrate supplied by AMG had a sheet resistance of 14.18 Ω/sq, which was deposited at 270°C. After that, PEDOT:PSS (AI4083) was spin-coated on the ITO/Ag/ITO and ITO anodes, which were subsequently annealed at 120°C for 10 min in air. Then, a blend of P3HT (25 mg, Rieke Metals) and PCBM (25 mg, Nano-C) in 1,2-dichlorobenzene (2 ml) was spin-coated onto the PEDOT:PSS layer in a nitrogen-filled glove box. After that a solvent-annealing treatment was performed by keeping the

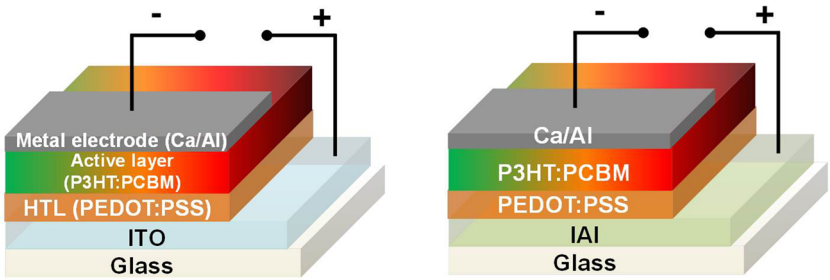

Fig. 1. Schematic diagrams of OSCs consisting of substrate, transparent electrode, a hole transport layer, an active layer, and cathode electrode.

photoactive films inside a covered glass jar for 120 min, and each sample was subsequently annealed at 110°C for 10 min. The organic layer-coated samples were rapidly transferred to a glove box to avoid water condensation. Finally, a Ca/Al cathode (20 nm/100 nm) (4.65 mm^2) was deposited on the photoactive layer by a thermal evaporator. The Ca/Al cathode layer was patterned by a shadow metal mask. All organic and cathode layers on the ITO/Ag/ITO and ITO anodes were all at once coated by the same coating processes. The photocurrent density–voltage (J–V) characteristics of OSCs fabricated with ITO/Ag/ITO and ITO electrodes were examined using a Keithley 2400 source measure unit under 100 mW/cm^2 illumination with AM 1.5 G irradiation from a solar simulator.

RESULTS AND DISCUSSION

Figure 2 shows the XRD patterns obtained from ITO-only (150 nm) and ITO/Ag (19 nm)/ITO multilayer films as a function of ITO thickness (d_{ITO}). The ITO-only layer has peaks at 2θ = 21.4°, 30.5°, 35.4°, 37.6°, 41.8°, 45.6°, 51.0°, 55.9°, and 62.1° that correspond to the (211), (222), (400), (411), (332), (431), (440), (611), and (622) planes, respectively (JCPDS No. 71-2195). It is noted that the ITO-only layer exhibits a very strong (222) peak, which can be attributed to the texturing of ITO.[22] Except for the 17-nm-thick ITO multilayer sample, the ITO/Ag/ITO samples have peaks at 2θ = 21.4°, 30.5°, 35.4°, 37.6°, 51.0°, and 62.1° that correspond to the (211), (222), (400), (411), (440) and (622) planes of ITO, respectively (JCPDS No. 71-2195). However, the peaks are slightly shifted towards the lower-angle side. Although the exact mechanism for this behavior is not clearly understood at the moment, it may be attributed to the facts that the multilayer ITO layer is much thinner than the ITO-only layer and the middle Ag layer is inserted between the ITO layers. For the ITO/Ag/ITO samples, there are additional peaks at 2θ = 38.3° and 64.6° that correspond to the (111) and (220) plane of Ag (JCPDS No. 87-0720). Despite the low deposition temperature, the ITO films show crystalline characteristics, which could be ascribed to the crystalline transition temperature ($T/T_m <$ 0.19–150°C) of ITO films.[23,24] It is noted that the 17-nm and 33-nm-thick ITO multilayer films show fewer crystalline peaks than other multilayer samples. The intensity of the (400) peak of ITO increases with increasing ITO thickness; this is due to the increased ITO thickness.

Figure 3 shows the optical transmittance obtained from the ITO-only (150 nm) and ITO/Ag (19 nm)/ITO multilayer films as a function of d_{ITO}. The conventional ITO-only film shows an optical transmittance of 96.5% at a wavelength of 530 nm. For the ITO/Ag (19 nm)/ITO samples, the transmittance reaches an overall maximum and then gradually decreases with increasing wavelength. The transmittance at 530 nm is measured to be 69.7%, 84%, 90%, 73.2%, and 46.5% for the 17 nm, 33 nm, 50 nm, 67 nm, and 83 nm-thick samples, respectively. The transmission window (full width half maximum) slightly widens and gradually shifts toward lower energies as d_{ITO} increases. It is noted that the 83-nm-thick sample shows a broad transmission minimum at ~415 nm. This could be attributed to interference between reflective partial waves.[25]

Figure 4 exhibits the carrier concentration and Hall mobility of the ITO/Ag (19 nm)/ITO multilayer films as a function of d_{ITO}. The ITO-only film gave a carrier concentration of 8.46×10^{20} cm^{-3}. For the multilayer samples, the carrier concentration moderately decreases from 2.01×10^{22} to 7.20×10^{21} cm^{-3} as d_{ITO} increases from 17 nm to 83 nm. The decrease in carrier concentration with increasing ITO thickness can be explained as follows. The 19-nm thick metallic Ag layer makes a major contribution to the carrier concentration. Compared with conventional ITO electrode with a sheet resistance of 14.18 Ω/sq. that was deposited at 270°C, the room-temperature-deposited ITO (in O/M/O) had much higher sheet resistance. For example, room-temperature-deposited ITO (100 nm thick) had a sheet resistance of 175.99 Ω/sq. Thus, an increase in the thickness of room-temperature-deposited resistive ITO would result in a reduction in the carrier concentration (Fig. 4) because the volume fraction of Ag in the ITO/Ag/ITO layer decreases with increasing ITO thickness. The mobility of the ITO-only sample was 44.97 cm^2/Vs. For the multilayer samples, the mobility varies from 18.12 to

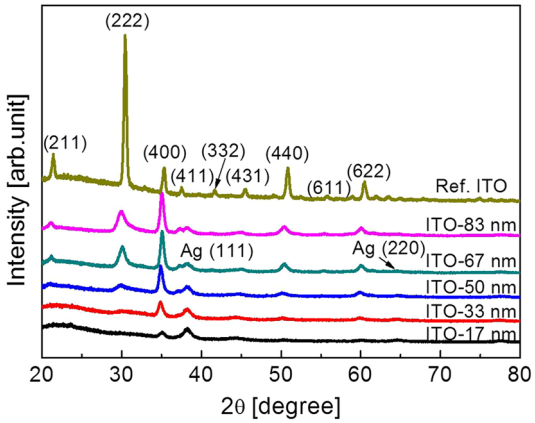

Fig. 2. XRD patterns obtained from a reference ITO and ITO/Ag (19 nm)/ITO multilayer films as a function of ITO layer thickness.

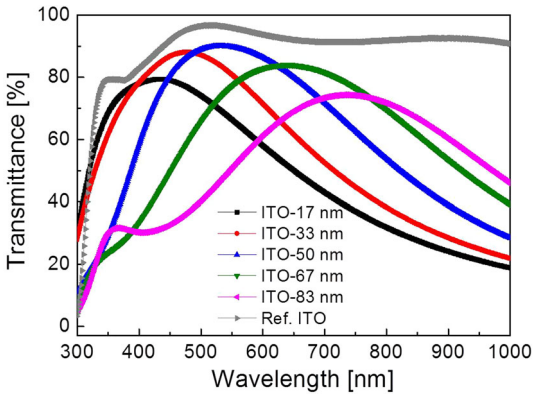

Fig. 3. Transmittance spectra of ITO and ITO/Ag (19 nm)/ITO multilayer films various ITO layer thicknesses.

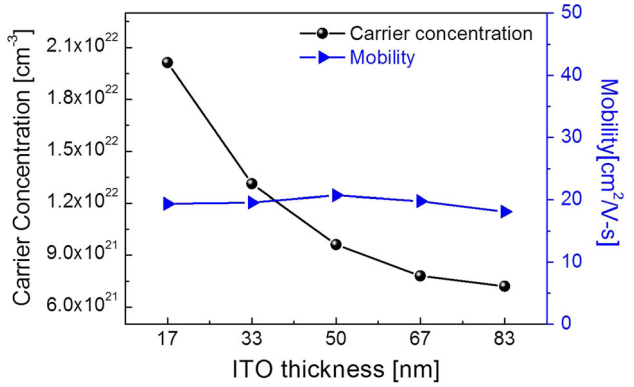

Fig. 4. Carrier concentration and Hall mobility of ITO/Ag (19 nm)/ITO multilayer films with various ITO layer thicknesses.

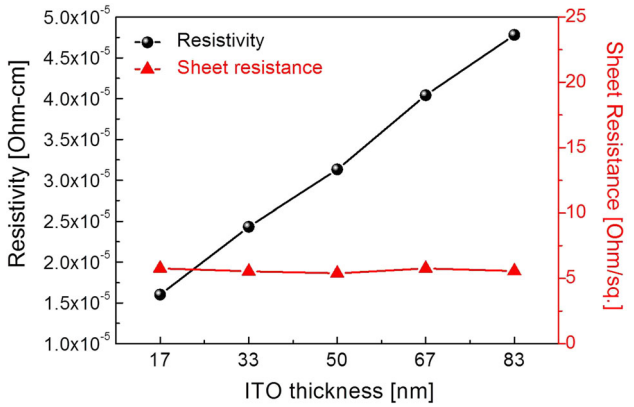

Fig. 5. Sheet resistance and resistivity of ITO/Ag (19 nm)/ITO multilayer films with various ITO layer thicknesses.

20.72 cm^2/Vs with the ITO thickness. Because the Ag thickness is constant, the mobility characteristics may be explained by the dominant contribution of interface scattering.[26]

Figure 5 shows the sheet resistance and resistivity of the ITO/Ag (19 nm)/ITO multilayer films as a function of d_{ITO}. The ITO-only sample had a sheet resistance of 14.18 Ω/sq. The multilayer samples exhibit low sheet resistances ranging from 5.40 to 5.78 Ω/sq. The ITO-only sample exhibited a resistivity of 1.63×10^{-4} Ω-cm. For the multilayer samples, the resistivity increases from 1.60×10^{-5} to 4.78×10^{-5} Ω-cm as d_{ITO} increases from 17 nm to 83 nm. The resistivity is inversely proportional to the mobility and the carrier concentration.[27] Thus, with the fact that the mobility slightly varies with increasing d_{ITO}, this indicates that the resistivity could be dominated by the carrier concentration.

Figure 6 shows calculated Haacke's FOMs (φ_{TC}) of the ITO/Ag (19 nm)/ITO multilayer films as a function of d_{ITO}. FOMs (φ_{TC}) was calculated using the equation, $\varphi_{TC} = T_{av}^{10}/R_s$ Ref. 28, where R_s is the sheet resistance and T_{av} is the average optical transmittance in the range 450–750 nm. T_{av} can be estimated using the relation, $T_{av} = \int v(\lambda)T(\lambda)d(\lambda)/\int v(\lambda)d(\lambda)$, where $T(\lambda)$ is the transmittance and $v(\lambda)$ is the photopic luminous efficiency function defining the standard observer for photometry.[29] φ_{TC} increases, reaches a maximum at 50 nm and then decreases as d_{ITO} increases. The 50 nm-thick ITO multilayer sample exhibits a maximum φ_{TC} of 51.89×10^{-3} Ω^{-1}. As d_{ITO} varies, the sheet resistance slightly changes from 5.40 to 5.78 Ω/sq., while the transmittance at 530 nm varies from 46.5% to 90%. This denotes that φ_{TC} can be dominated by the contribution of transmittance. Note that the ITO (50 nm)/Ag (19 nm)/ITO (50 nm) multilayer sample gives higher φ_{TC} than the ITO-only film (43.06×10^{-3} Ω^{-1}). Considering the fact that the ITO-only showed higher transmittance than the ITO/Ag/ITO sample, the higher φ_{TC} can be attributed to the dominant contribution of the lower sheet resistance.

Figure 7 illustrates a surface morphology of the ITO (50 nm)/Ag (19 nm)/ITO (50 nm) multilayer film. The AFM image reveals a uniform surface without cracks or pits. The surface is smooth with a root mean square (RMS) roughness of 0.49 nm. For OSCs, the organic layers (HTL; PEDOT:PSS, active layer; P3HT:PCBM) are spin-coated on the

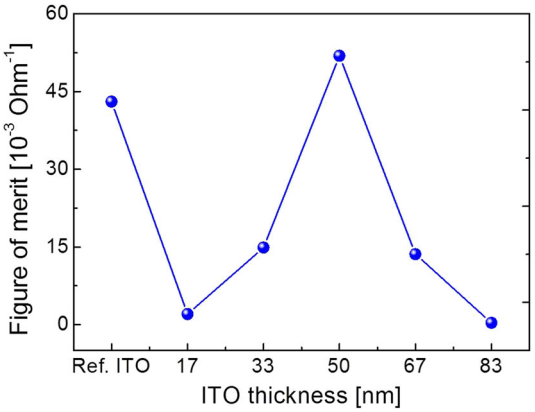

Fig. 6. Calculated Haacke's FOMs (φ_{TC}) of ITO/Ag (19 nm)/ITO multilayer films as a function of ITO layer thickness.

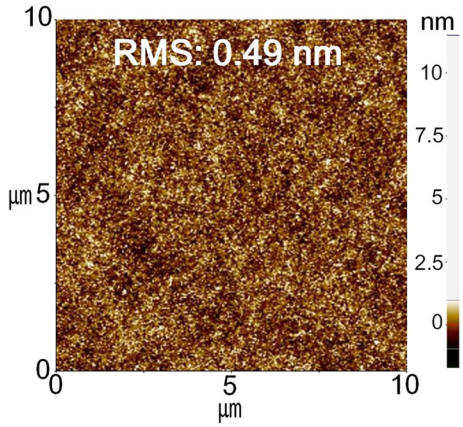

Fig. 7. An AFM image obtained from an ITO/Ag/ITO (50 nm/19 nm/50 nm) multilayer film.

electrode, and; hence, the smoothness of the electrode is critical. In other words, the smooth surface of the underlying electrode is vital for the uniform deposition of the organic layers, because the performance of OSCs is sensitively affected by the uniformity of the electrode.

Figure 8 shows the current density–voltage (J–V) curves obtained from P3HT:PCBM BHJ-based OSCs fabricated with conventional ITO-only and optimized ITO (50 nm)/Ag (19 nm)/ITO (50 nm) anode electrodes. The inset shows the device structure. A PCE of the OSCs can be given as[30]:

$$\mathrm{PCE} = \frac{\mathrm{P_{out}}}{\mathrm{P_{in}}} = \frac{V_{OC} J_{SC} FF}{\mathrm{P_{in}}}, \qquad (1)$$

where P_{out} is the power output of a device, P_{in} is the power of incident light source (mW/cm^2), V_{OC} is open-circuit voltage, J_{SC} is short-circuit current density, and FF is the fill factor. PCE and other parameters are estimated. The ITO-based OSCs show J_{SC} = 9.01 mA/cm^2, V_{OC} = 0.63 V, FF = 61.62%, and PCE = 3.48%. On the other hand, the ITO/Ag/ITO-based OSCs give J_{SC} = 7.40 mA/cm^2, V_{OC} = 0.62 V, FF = 62.19%, and PCE = 2.84%.

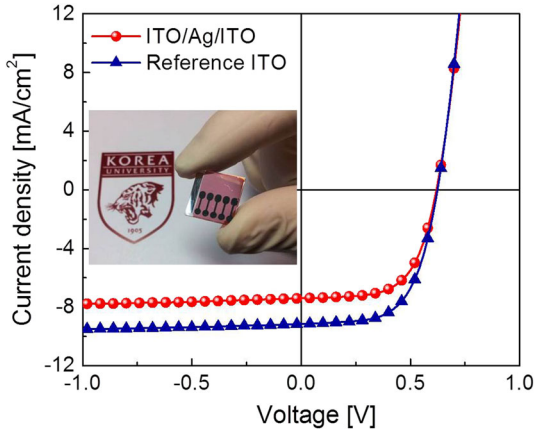

Fig. 8. J–V curves obtained from P3HT:PCBM BHJ-based OSCs fabricated with reference ITO-only and optimal ITO/Ag/ITO electrodes. The inset shows a device structure.

Because FF sensitively depends on the sheet resistance of electrodes,[31] the higher FF of the ITO/Ag/ITO-based OSCs could be ascribed to the lower sheet resistance (5.4 Ω/sq).

Although the ITO/Ag/ITO electrode showed higher FOM than the conventional ITO-only electrode, the ITO/Ag/ITO-based OSCs did not produce better performance than the ITO-based OSCs. This may be explained in terms of inferior mobility (18.12–20.72 cm^2/Vs) which is much lower than that of the ITO-only sample (44.97 cm^2/Vs) (Fig. 4). The lower mobility could be due to the different interface characteristics and crystal quality. In other words, unlike the ITO-only electrode, there are additional interfaces, such as oxide/Ag and Ag/oxide, which may serve as scattering centers for carriers. In addition, as shown for the XRD results (Fig. 2), the crystal quality of the oxide films was not better than the high-temperature-deposited ITO-only film. Therefore, if the deposition conditions for the ITO/Ag/ITO electrode are best optimized, better performance would be realized. This is particularly true for flexible OSCs, where high-temperature depositions are not allowed; the current ITO-only films were deposited at 270°C. Therefore, with the facts that OSCs with ITO/Ag/ITO electrode show PCEs comparable to that of OSCs with an ITO electrode and the ITO/Ag/ITO was deposited at room temperature; these imply that the optimal ITO/Ag/ITO electrode can be a potentially important electrode for flexible display devices, to which a high-temperature-deposited conventional ITO electrode cannot be applied.

SUMMARY AND CONCLUSIONS

The electrical and optical properties of ITO/Ag (19 nm)/ITO multilayer films were characterized as a function of ITO thickness for use as an anode in OSCs. The ITO/Ag/ITO multilayer films showed lower sheet resistances than a conventional ITO-only layer. The transmission window slightly

widened and shifted toward lower energies with increasing ITO thickness. The ITO/Ag/ITO (50 nm/19 nm/50 nm) film showed somewhat lower transmittance than the ITO-only layer. The ITO/Ag/ITO (50 nm/19 nm/50 nm) film gave higher FOM than the ITO-only layer. P3HT:PCBM BHJ-based OSCs fabricated with the ITO (50 nm)/Ag (19 nm)/ITO (50 nm) yielded a PCE of 2.84%, while that with a commercial ITO-only anode produced 3.48%. This indicates that the optimal ITO/Ag/ITO multilayer films can be a reliable transparent conducting electrode for use in flexible display applications.

ACKNOWLEDGEMENTS

This work was supported by the Korea Evaluation Institute of Industrial Technology (KEIT) (Grant No. 10049601) and the world class 300 project (Grant No. S2317456) of the Small and Medium Business Administration (Korea).

REFERENCES

1. N.S. Sariciftci, L. Smilowitz, A.J. Heeger, and F. Wudl, *Science* 258, 1474 (1992).
2. G. Yu, J. Gao, J.C. Hummelen, F. Wudl, and A.J. Heeger, *Science* 270, 1789 (1995).
3. C.J. Brabec, N.S. Sariciftci, and J.C. Hummelen, *Adv. Funct. Mater.* 11, 15 (2001).
4. A.A. Bakulin, A. Rao, V.G. Pavelyev, P.H.M. Loosdrecht, M.S. Pshenichnikov, D. Niedzialek, J. Cornil, D. Beljonne, and R.H. Friend, *Science* 332, 1340 (2011).
5. L. Dou, J. You, J. Yang, C.-C. Chen, Y. He, S. Murase, T. Moriarty, K. Emery, G. Li, and Y. Yang, *Nat. Photonics* 6, 180 (2012).
6. P. Kuang, J.-M. Park, W. Leung, R.C. Mahadevapuram, K.S. Nalwa, T.-G. Kim, S. Chaudhary, K.-M. Ho, and K. Constant, *Adv. Mater.* 23, 2469 (2011).
7. V. Kumar and H. Wang, *Sol. Energy Mater. Sol. Cells* 113, 179 (2013).
8. D.H. Apaydın, D.E. Yıldız, A. Cirpan, and L. Toppare, *Sol. Energy Mater. Sol. Cells* 113, 100 (2013).
9. G. Segev, A. Kribus, and Y. Rosenwaks, *Sol. Energy Mater. Sol. Cells* 113, 114 (2013).
10. F. Steuber, J. Staudigel, M. Stossel, J. Simmerer, and A. Winnacker, *Appl. Phys. Lett.* 74, 3558 (1999).
11. J. Cui, A. Wang, N.L. Edleman, J. Ni, P. Lee, N.R. Armstrong, and T. Marks, *Adv. Mater. (Weinheim, Ger.)* 13, 1476 (2001).
12. R.B.H. Tahar, T. Ban, Y. Ohya, and Y. Takahashi, *J. Appl. Phys.* 83, 2631 (1998).
13. S. Yu, W. Zhang, L. Li, D. Xu, H. Dong, and Y. Jin, *Acta Mater.* 61, 5429 (2013).
14. A. Dhar and T.L. Alford, *J. Appl. Phys.* 112, 103113 (2012).
15. M. Makha, L. Cattin, Y. Lare, L. Barkat, M. Morsli, M. Addou, A. Khelil, and J.C. Bernède, *Appl. Phys. Lett.* 101, 233307 (2012).
16. J.H. Kim, H.-K. Lee, J.-Y. Na, S.-K. Kim, Y.-Z. Yoo, and T.-Y. Seong, *Curr. Appl. Phys.* 15, 452 (2015).
17. T.H. Kim, C.H. Kim, S.K. Kim, Y.S. Lee, and L.S. Park, *Mol. Cryst. Liq. Cryst.* 532, 112 (2010).
18. K.H. Choi, J.Y. Kim, Y.S. Lee, and H.J. Kim, *Thin Solid Films* 341, 152 (1999).
19. T.H. Kim, B.H. Choi, J.S. Park, S.M. Lee, Y.S. Lee, and L.S. Park, *Mol. Cryst. Liq. Cryst.* 520, 209 (2010).
20. H.-J. Kim, K.-W. Seo, Y.H. Kim, J. Choi, and H.-K. Kim, *Appl. Surf. Sci.* 328, 215 (2015).
21. J.H. Kim, T.-W. Kang, S.-I. Na, Y.-Z. Yoo, and T.-Y. Seong, *Curr. Appl. Phys.* 15, 829 (2015).
22. P. Thilakan, C. Minarini, S. Loreti, and E. Terzini, *Thin Solid Films* 388, 34 (2001).
23. Y.-S. Park, H.-K. Park, S.-W. Cho, J.-A. Jeong, K.-H. Choi, H.-K. Kim, J.-Y. Lee, J.-H. Lee, H.-D. Bae, and Y.-H. Tak, *Electrochem. Solid-State Lett.* 11, J85 (2008).
24. H.-K. Kim, D.-G. Kim, K.-S. Lee, M.-S. Huh, S.H. Jeong, K.I. Kim, and T.-Y. Seong, *Appl. Phys. Lett.* 86, 183503 (2005).
25. M.A. Kats, D. Sharma, J. Lin, P. Genevet, R. Blanchard, Z. Yang, M.M. Qazilbash, D.N. Basov, S. Ramanathan, and F. Capasso, *Appl. Phys. Lett.* 101, 221101 (2012).
26. A. Indluru and T.L. Alford, *J. Appl. Phys.* 105, 123528 (2009).
27. H. Han, J.W. Mayer, and T.L. Alford, *J. Appl. Phys.* 100, 083715 (2006).
28. G. Haacke, *J. Appl. Phys.* 47, 4086 (1976).
29. W.G. Driscoll and W. Vaughan, *Handbook of Optics* (USA: McGraw-Hill, 1978).
30. A. Luque and S. Hegedus, *Handbook of Photovoltaics Science and Engineering* (New York: Wiley, 2003).
31. Y.-Y. Choi, S.J. Kang, H.-K. Kim, W.M. Choi, and S.-I. Na, *Sol. Energy Mater. Sol. Cells* 96, 281 (2012).